Supplementary Information

Revealing the Crystalline Packing Structure of Y6 in the Active Layer of Organic Solar Cells: The Critical Role of Solvent Additives

Xinxin Xia, Le Mei, Chengliang He, Zeng Chen, Nannan Yao, Minchao Qin, Rui Sun, Zhenzhen Zhang, Yuyu Pan, Yiqun Xiao, Yuze Lin, Jie Min, Fengling Zhang, Haiming Zhu, Jean-Luc Bredas, Hongzheng Chen, Xian-Kai Chen*, and Xinhui Lu**

X. Xia, M. Qin, Y. Xiao, and Prof. X. Lu
Department of Physics, The Chinese University of Hong Kong, New Territories, Hong Kong
E-mail: xinhui.lu@cuhk.edu.hk

L. Mei, Y. Pan, and Prof. X.-K. Chen
Department of Chemistry, Department of Materials Science and Engineering, City University of Hong Kong, Kowloon, Hong Kong
Hong Kong Institute for Advanced Study, City University of Hong Kong, Hong Kong
E-mail: xche22@cityu.edu.hk

C. He and Prof. H. Chen
State Key Laboratory of Silicon Materials, MOE Key Laboratory of Macromolecular Synthesis and Functionalization, Department of Polymer Science and Engineering, Zhejiang University, Hangzhou, P. R. China
E-mail: hzchen@zju.edu.cn

Z. Chen and Prof. H. Zhu
Center for Chemistry of High-Performance & Novel Materials, Department of Chemistry, Zhejiang University, Hangzhou 310027, Zhejiang, China

N. Yao and Prof. F. Zhang
Department of Physics, Chemistry and Biology (IFM), Linköping University, Linköping, SE-58183, Sweden

R. Sun and Prof. J. Min
The Institute for Advanced Studies, Wuhan University, Wuhan 430072, China

Prof. J.-L. Bredas
Department of Chemistry and Biochemistry, The University of Arizona, Tucson, Arizona 85721-0088, USA

Z. Zhang and Prof. Y. Lin
Beijing National Laboratory for Molecular Sciences, CAS Key Laboratory of Organic Solids, Institute of Chemistry, Chinese Academy of Sciences, Beijing 100190, China

X. Xia and L. Mei contribute equally to this work.

Keywords: crystalline packing structure, Y6, device active layer, GIWAXS, solvent additives, molecular dynamics simulations

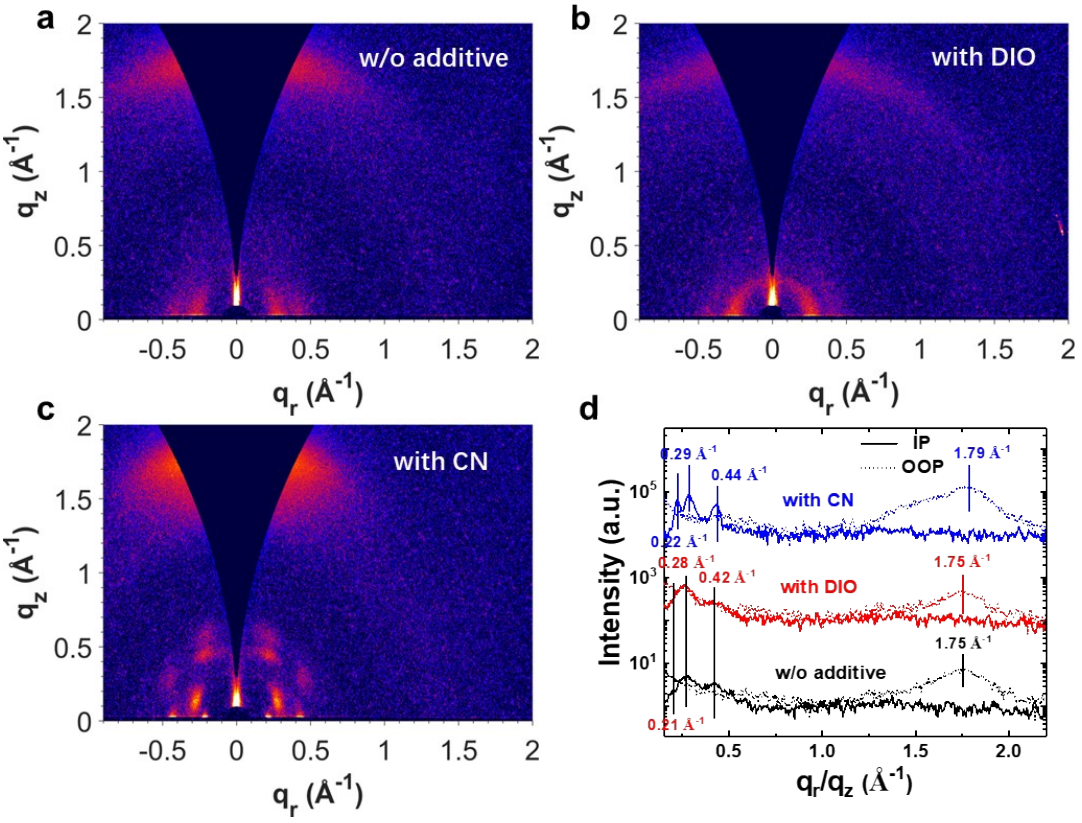

Figure S1. 2D GIWAXS patterns of Y6 neat films **(a)** without additive, **(b)** with 0.5vol% DIO and **(c)** with 0.5vol% CN. **(d)** Corresponding 1D linecuts. All the films are thermally annealed at 80 °C for 10 mins after spin coating.

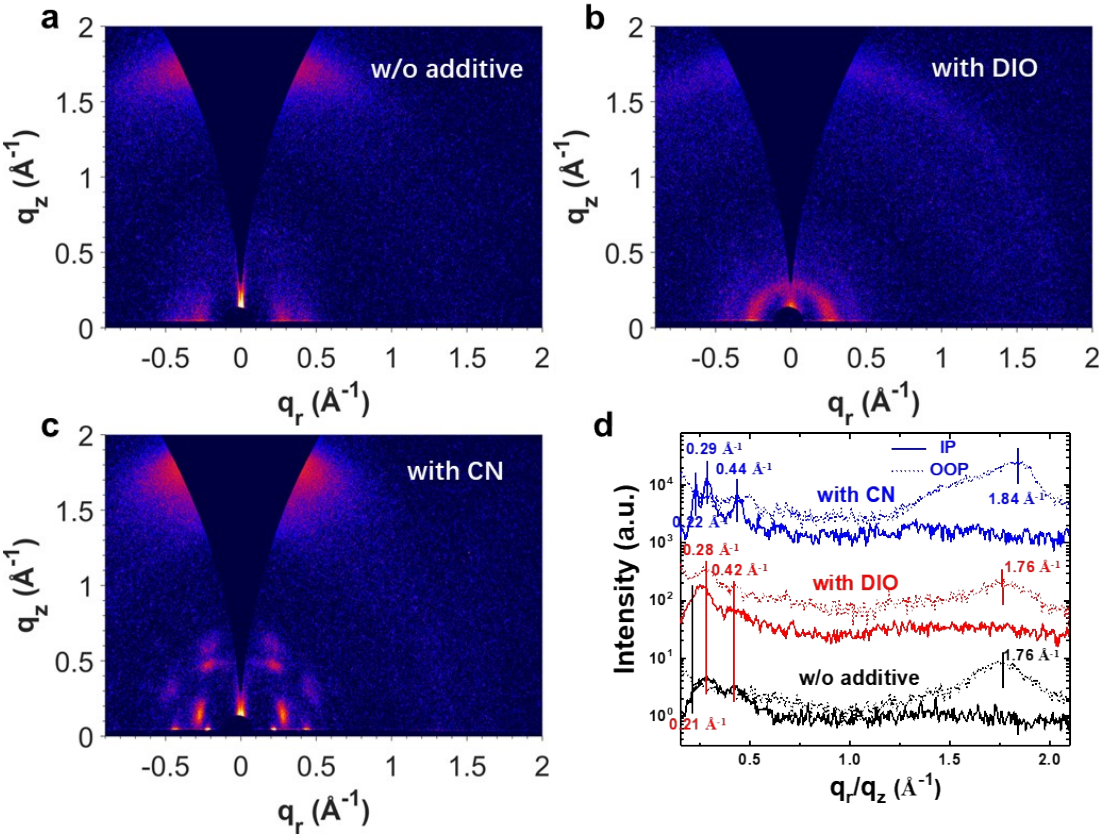

Figure S2. 2D GIWAXS patterns of Y6 neat films **(a)** without additive, **(b)** with 0.5vol% DIO and **(c)** with 0.5vol% CN. **(d)** Corresponding 1D linecuts. All the films are prepared without thermal annealing.

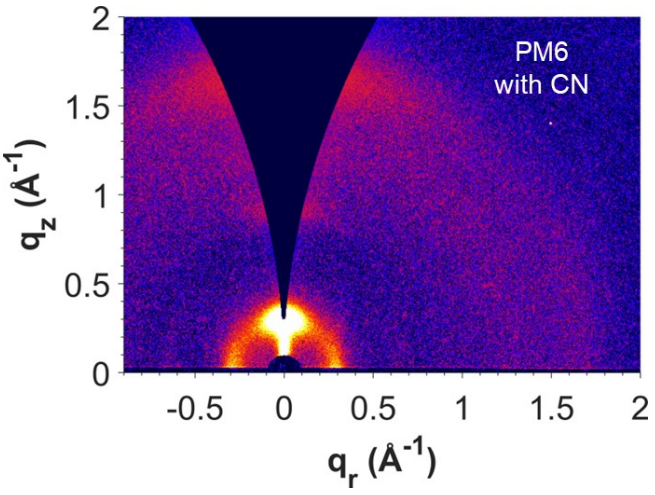

Figure S3. 2D GIWAXS pattern of a PM6 neat film prepared with 0.5vol% CN and thermal annealing at 80 °C for 10 mins.

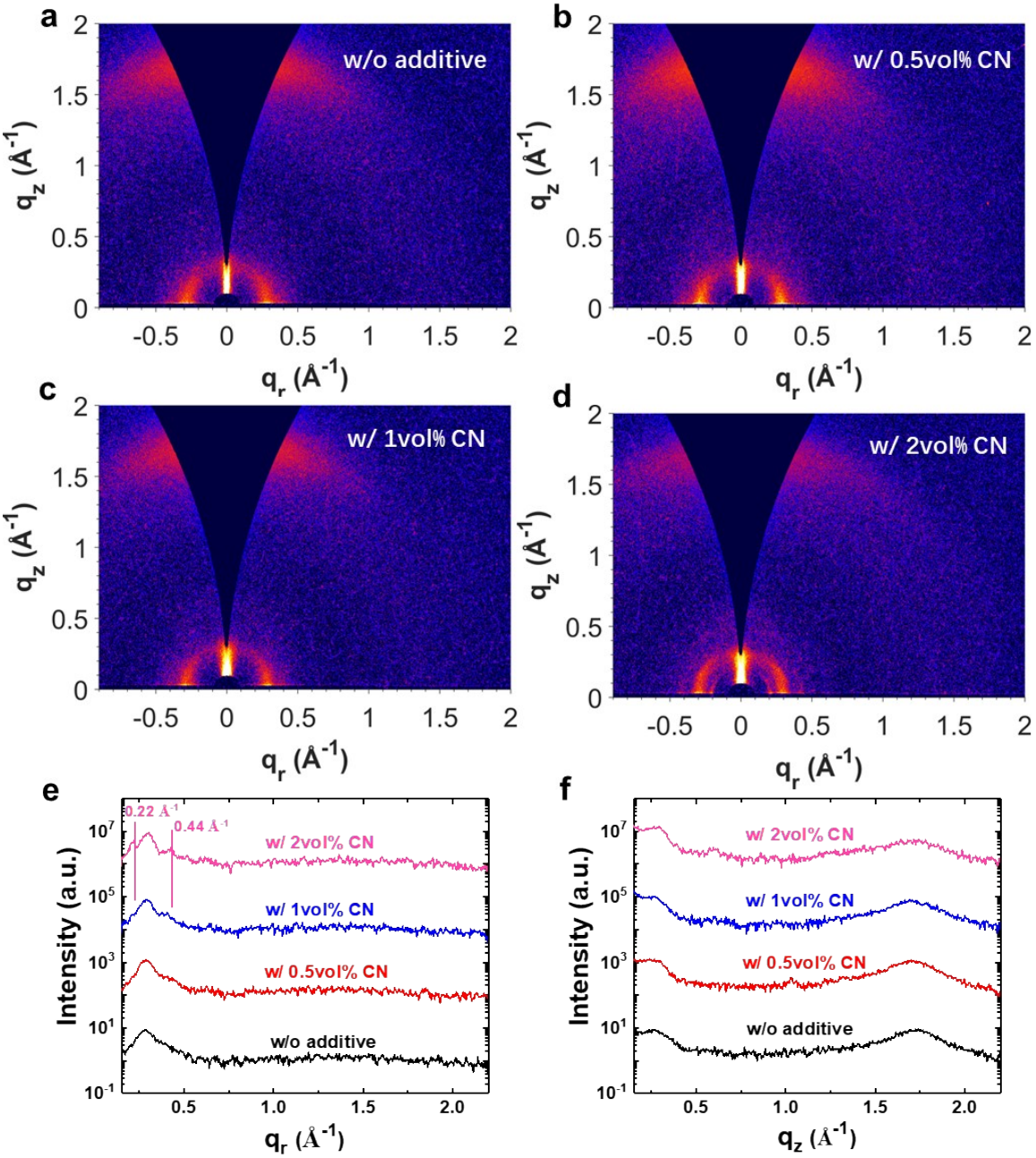

Figure S4. 2D GIWAXS patterns of PM6: Y6 blend films **(a)** without additive, **(b)** with 0.5vol% CN, **(c)** with 1vol% CN, and **(d)** with 2vol% CN. **(e-f)** Corresponding 1D linecuts. All the films are prepared with a D/A ratio of 1:1.2 and thermal annealing under 80 °C for 10 mins.

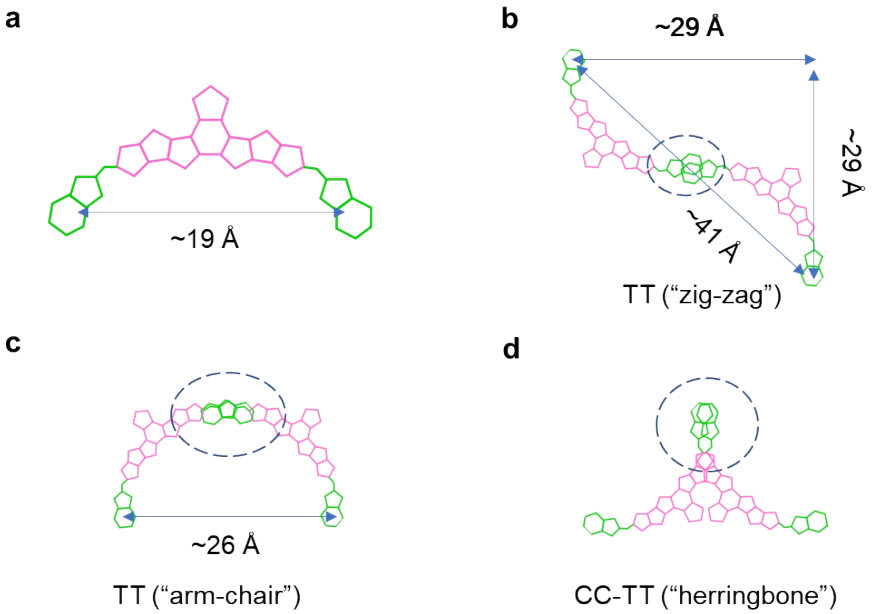

Figure S5. Illustration of **(a)** the single-molecule architecture and **(b-d)** various dimer configurations with different overlapping areas for Y6 (the alkyl chains are omitted for clarity).

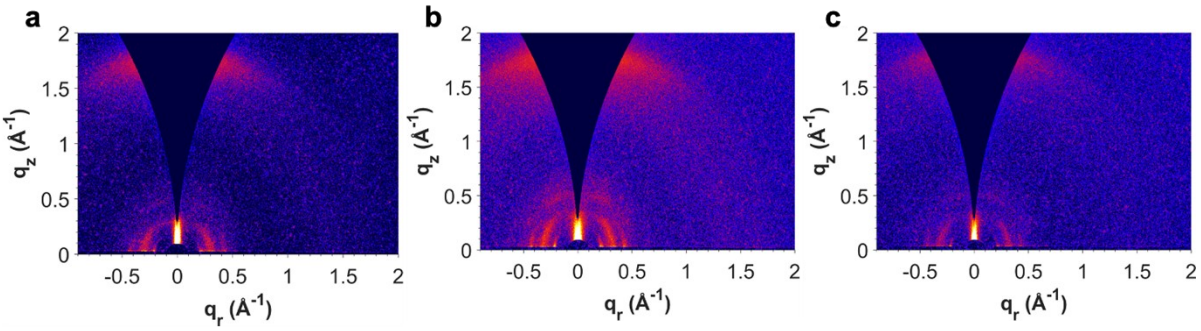

Figure S6. GIWAXS patterns of PM6:Y6 blend film (D/A=1:4, 0.5vol% CN) measured with various azimuth angles: **(a)** 0°, **(b)** 45°, **(c)** 90°. Note that variations of scattering intensities at different azimuth angles should be originated from the different lengths of footprint.

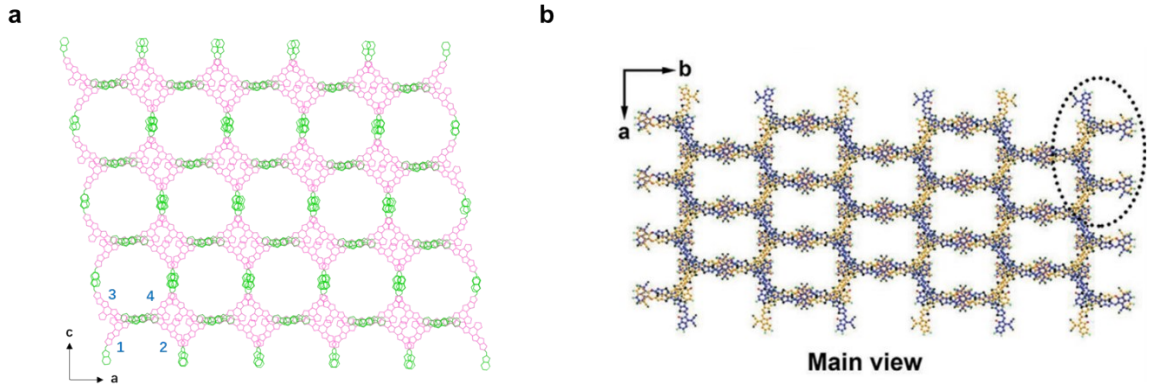

a = 29 Å, b = 16 Å, c = 29 Å, α = 90°, β = 90°, γ = 122°

a=23.701 Å, b=57.450 Å, c=14.396 Å, α=90°, β=118.541°, γ=90°

Figure S7. Top views of the crystalline structure of Y6 **(a)** in a thin film and **(b)** in the single crystal. [1, 2]

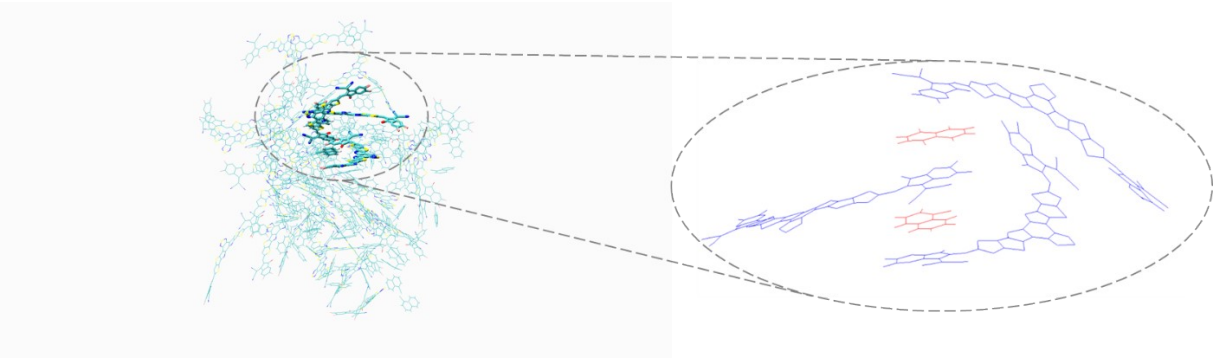

Figure S8. Illustration of the MDS results for Y6 with the CN additive at 300 K.

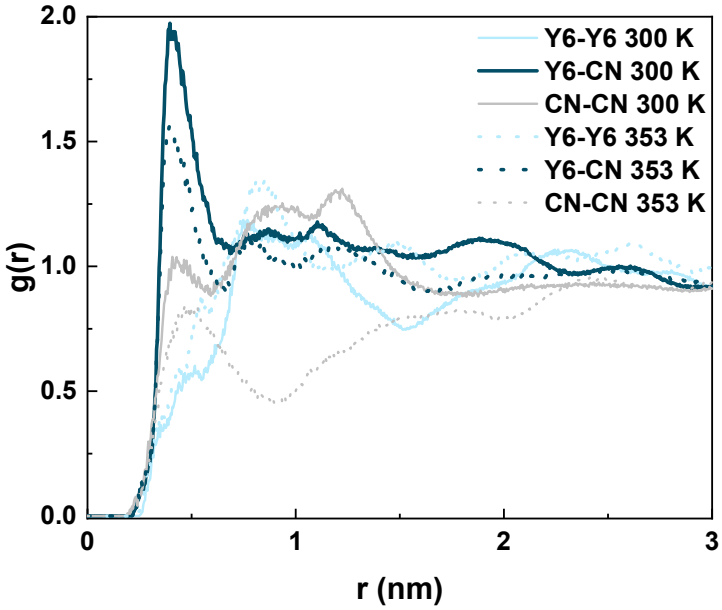

Figure S9. Radial distribution functions for Y6 with the CN additive at 300 and 353 K.

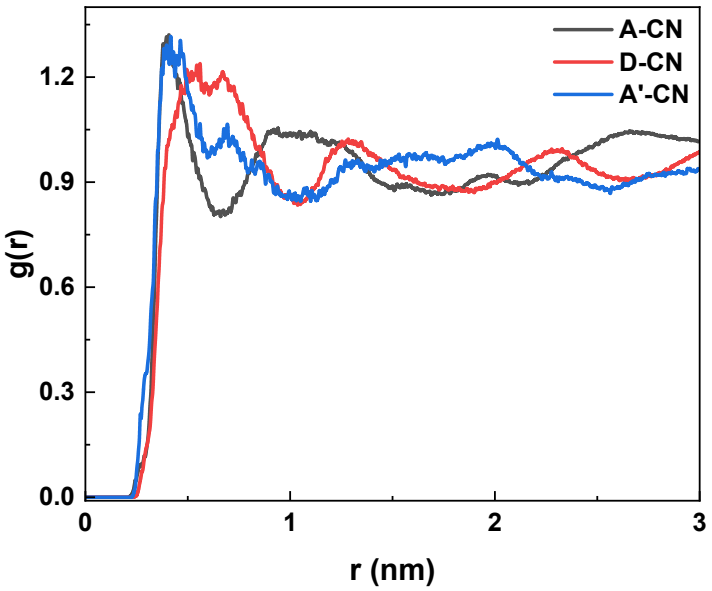

Figure S10. Radial distribution functions for the Y6 A and D moieties vs. CN at 300 K.

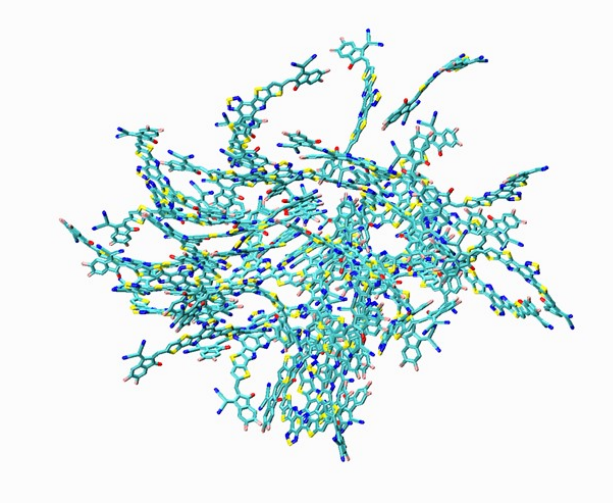

Figure S11. Illustration of the MDS results for pure Y6 at 300 K.

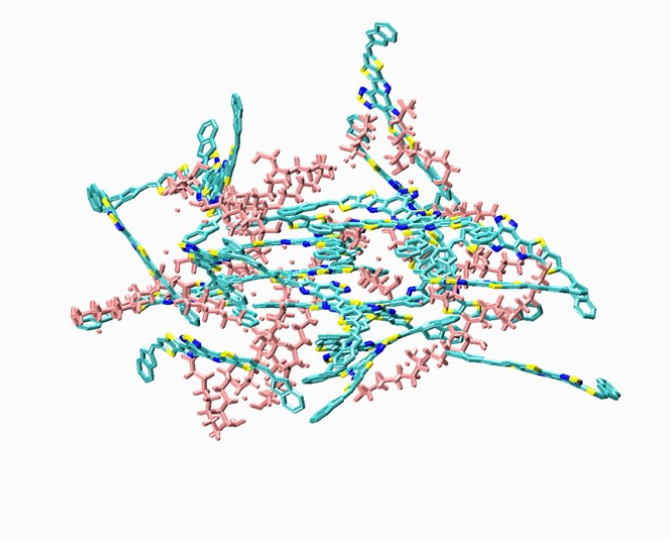

Figure S12. Illustration of the MDS results for Y6 (light green) with the DIO additive (light red) at 300 K.

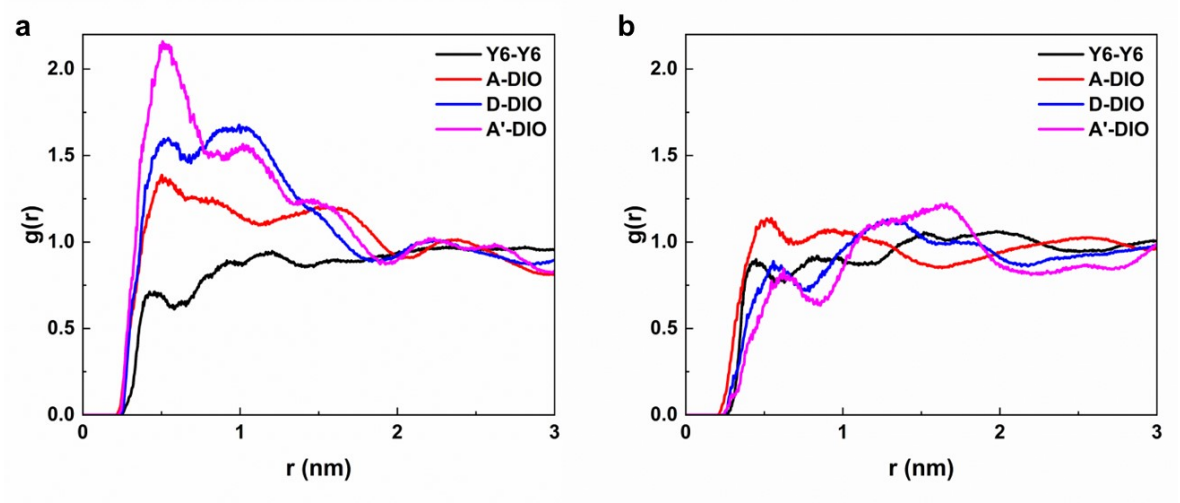

Figure S13. Radial distribution functions for Y6 and DIO at **(a)** 300 K and **(b)** 353 K.

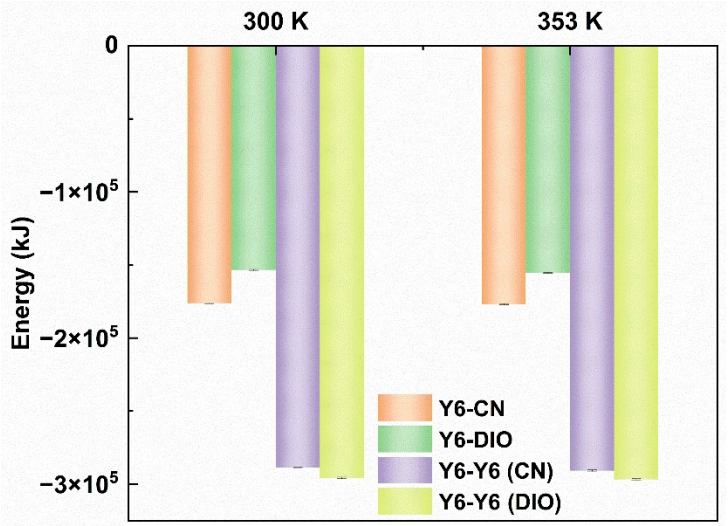

Figure S14. Interaction energies between the relevant molecules. The interaction energy is the sum of the blend system's electrostatics and van der Waals. For pristine Y6 film, the box included 300 Y6 molecules. However, the boxes contained 2078 additive CN and 600 Y6 molecules (total of 149604 atoms), and 1416 additive DIO and 600 Y6 molecules (total of 149016 atoms) for the hybrid systems. The ratios of Y6 to the additives are consistent with the experiment parameters.

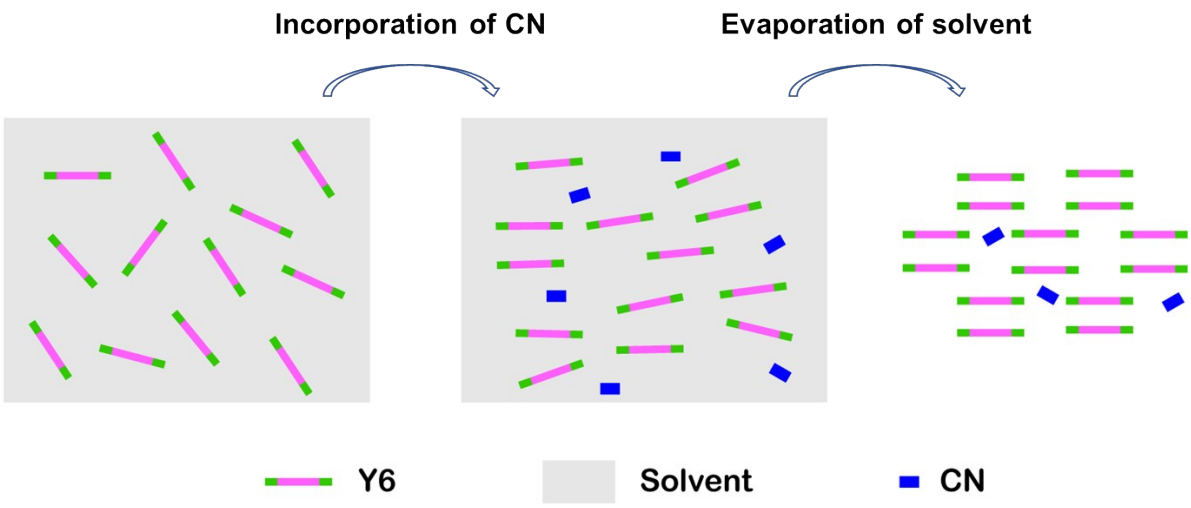

Figure S15. Schematic illustration of the impact of the CN additive on the crystallization of Y6.

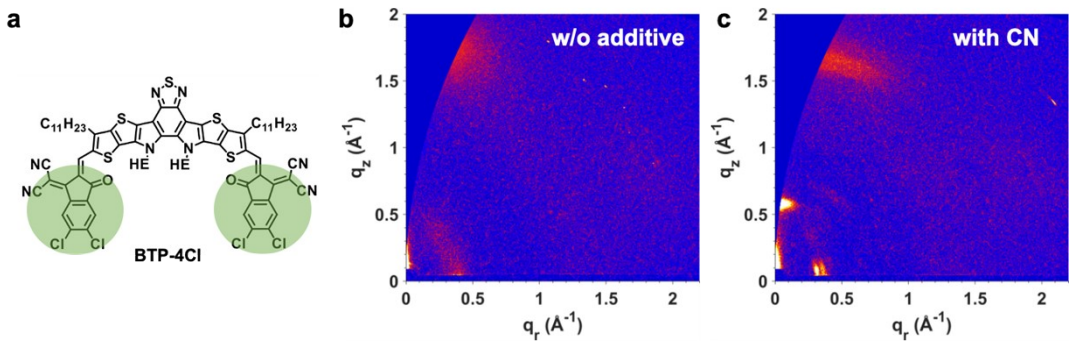

Figure S16. (a) Molecular structure of BTP-4Cl.[3] GIWAXS patterns of BTP-4Cl neat films **(b)** without additive and **(c)** with 0.5vol% CN.

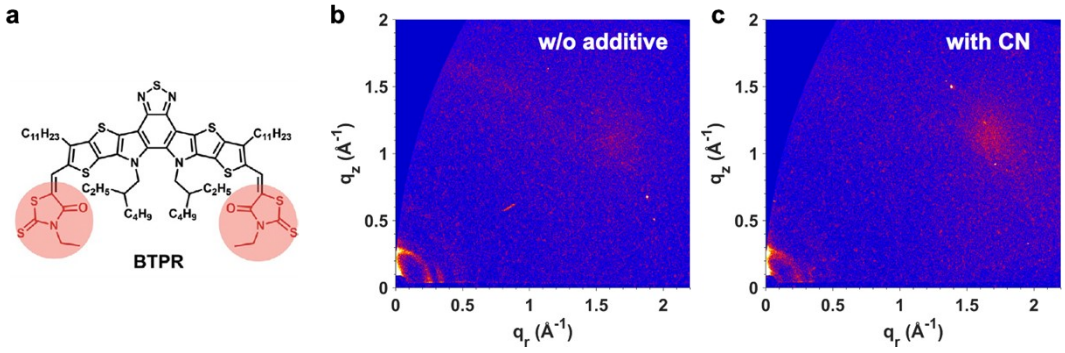

Figure S17. (a) Molecular structure of BTPR.[4] GIWAXS patterns of BTPR neat films **(b)** without additive and **(c)** with 0.5vol% CN.

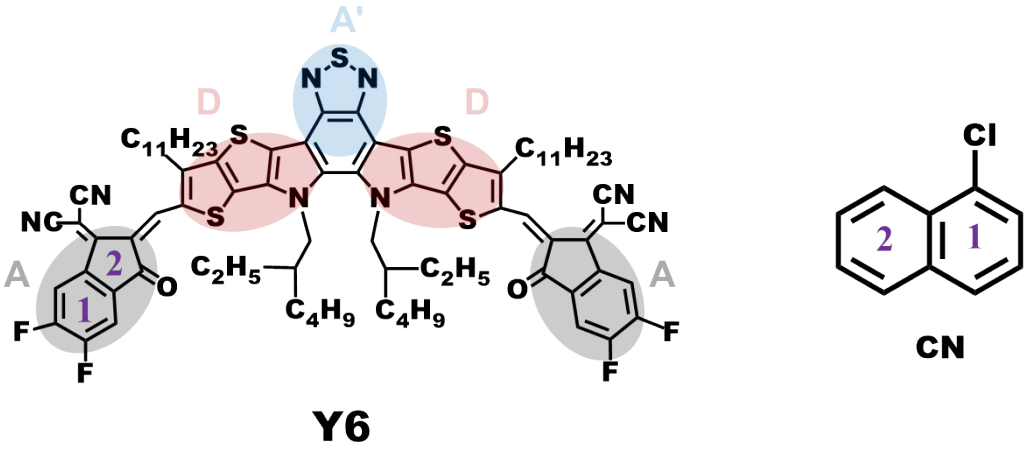

Figure S18. Labeling of the Y6 and CN moieties.

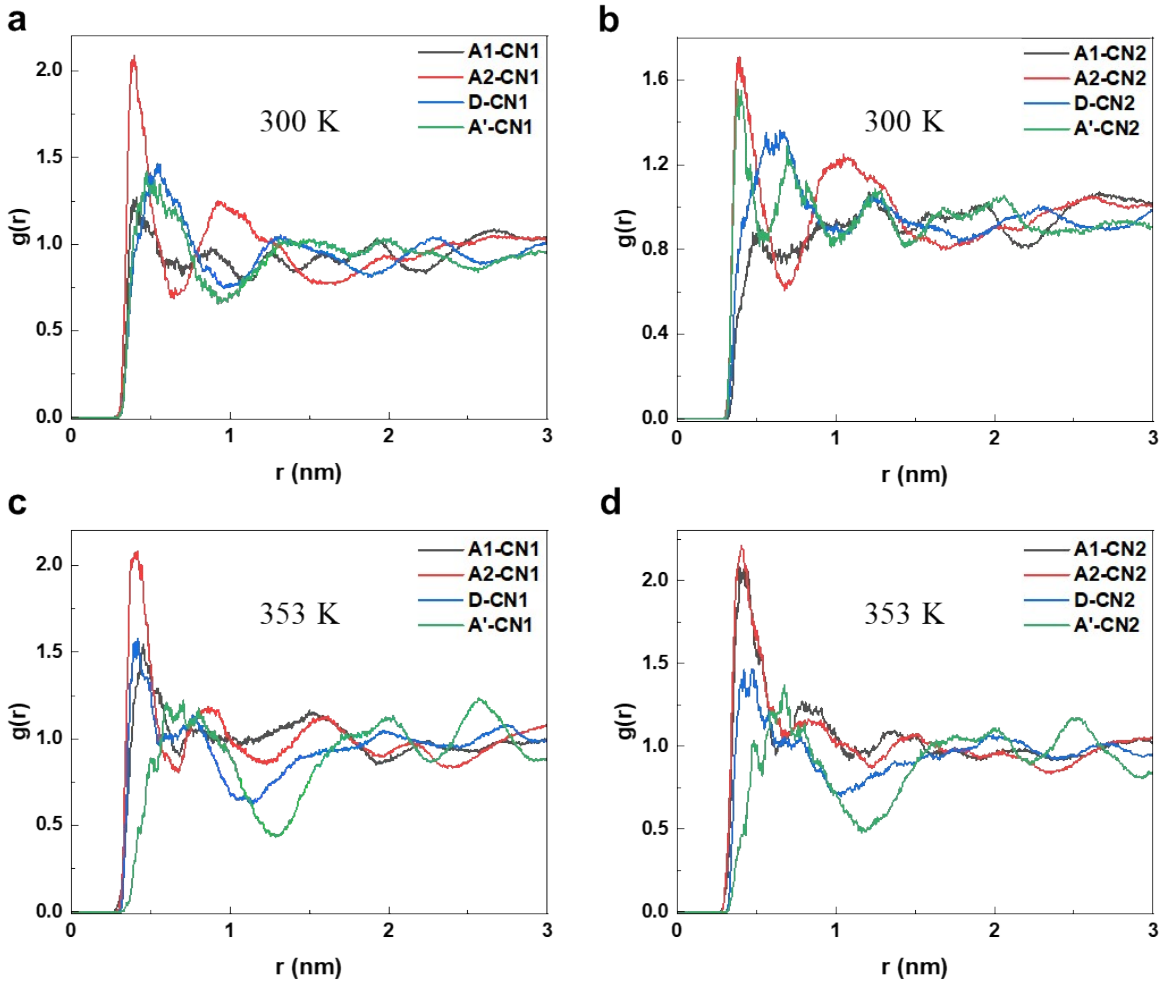

Figure S19. Radial distribution functions for the Y6 and CN moieties at **(a-b)** 300 K and **(c-d)** 353 K.

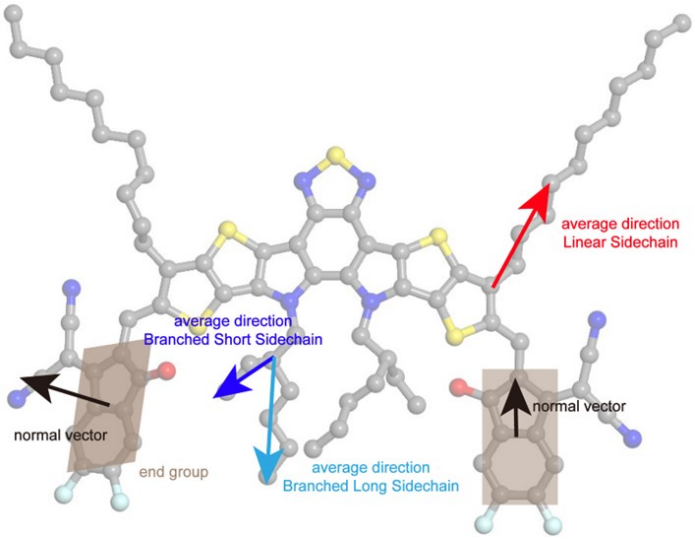

Figure S20. Illustration of the orientations of the end groups and linear and branched (long and short) side chains in the Y6 molecule.

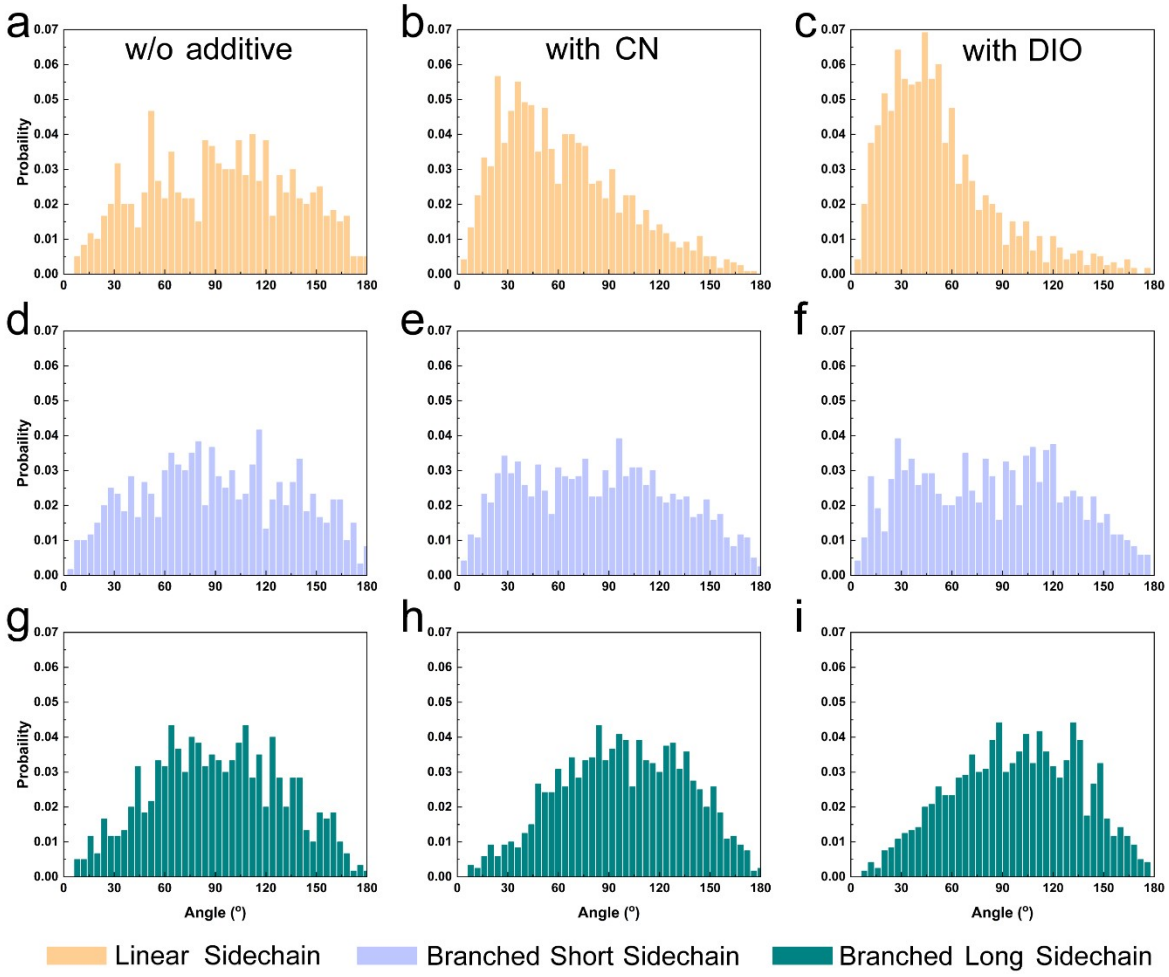

Figure S21. Distribution of the angles between the orientations of the end groups and various side chains for Y6 **(a, d, g)** without additive, **(b, e, h)** with CN, and **(c, f, i)** with DIO. The temperature is 300 K.

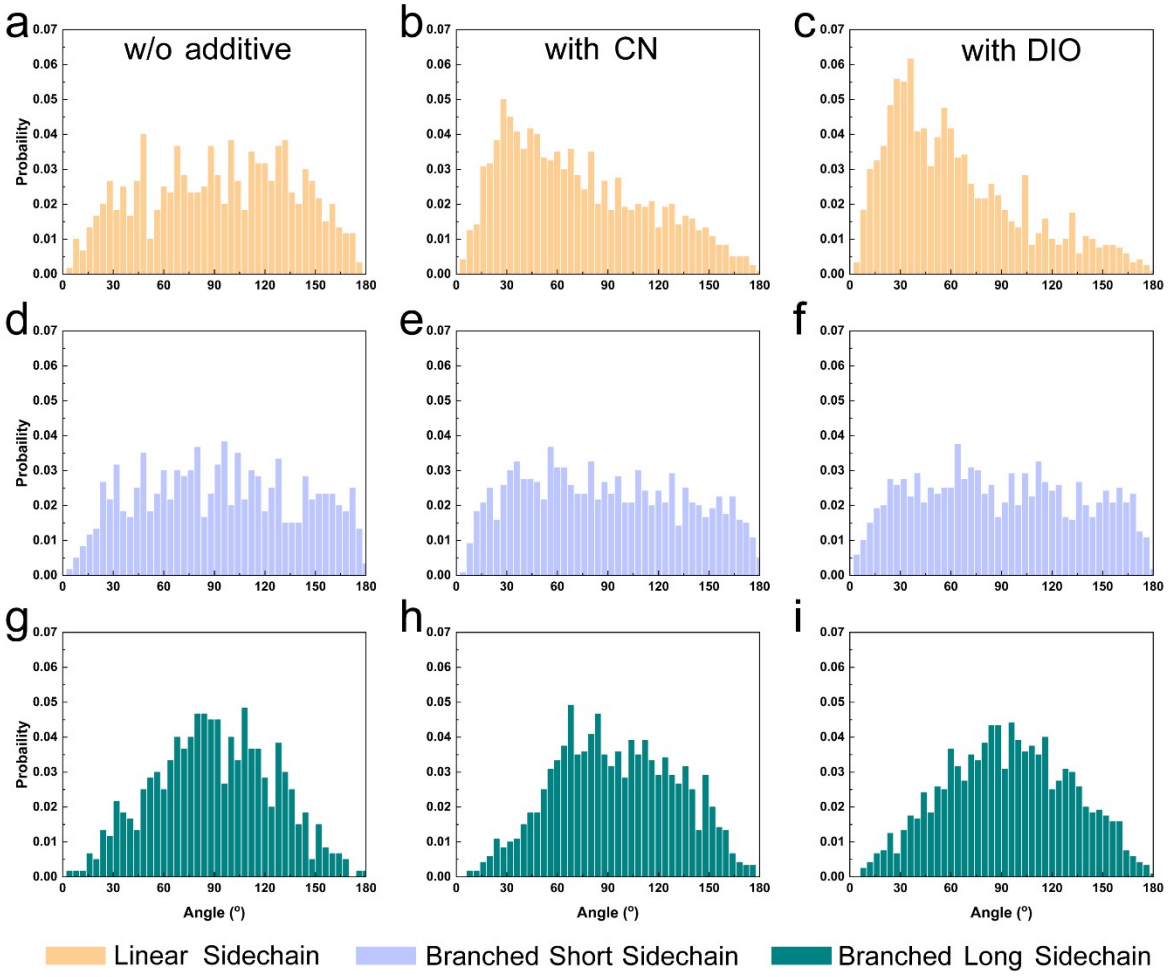

Figure S22. Distribution of the angles between the orientations of the end groups and various side chains for Y6 **(a, d, g)** without additive, **(b, e, h)** with CN, and **(c, f, i)** with DIO. The temperature is 353 K.

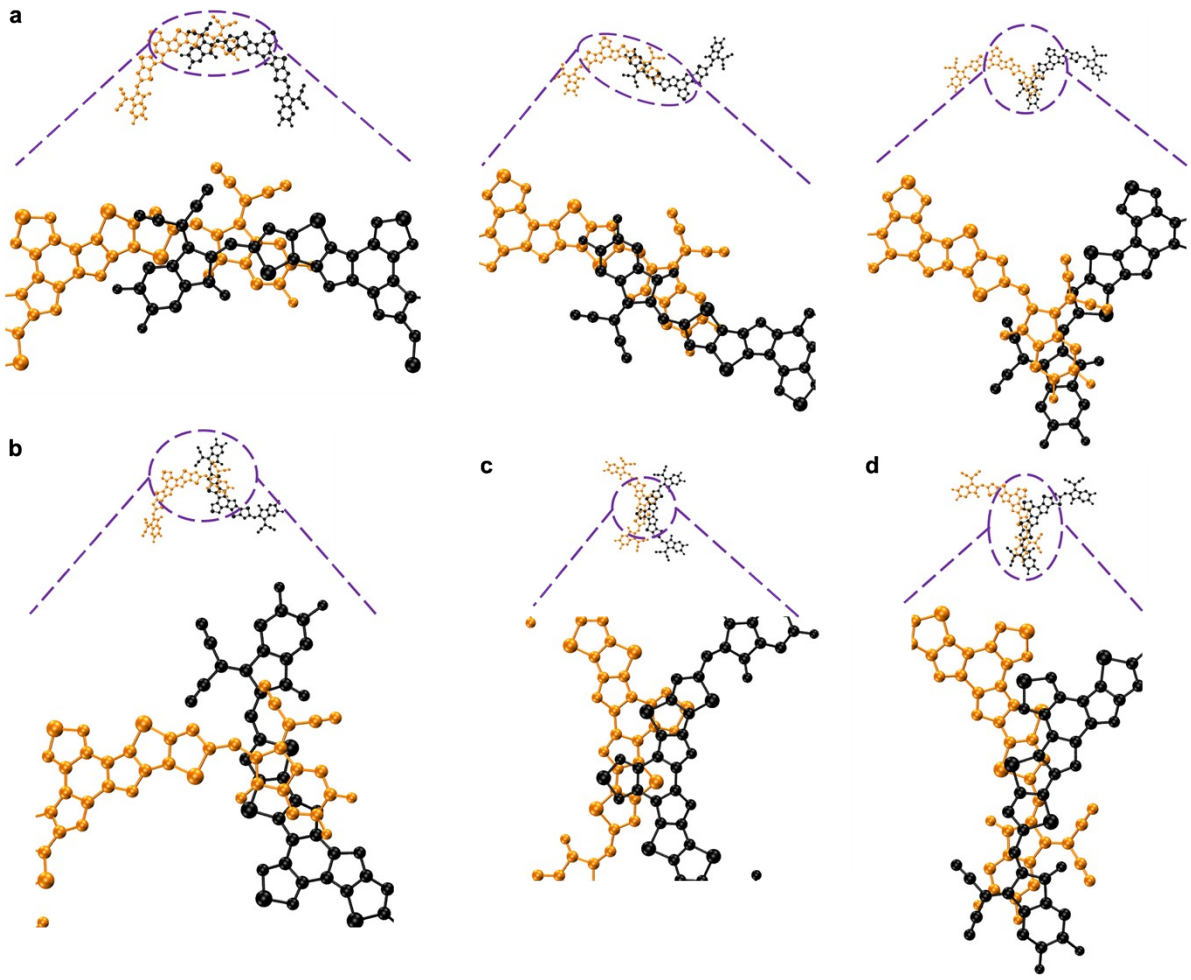

Figure S23. Enlargement of the interacting parts for **(a)** TT, **(b)** CT, **(c)** CC and **(d)** other dimers.

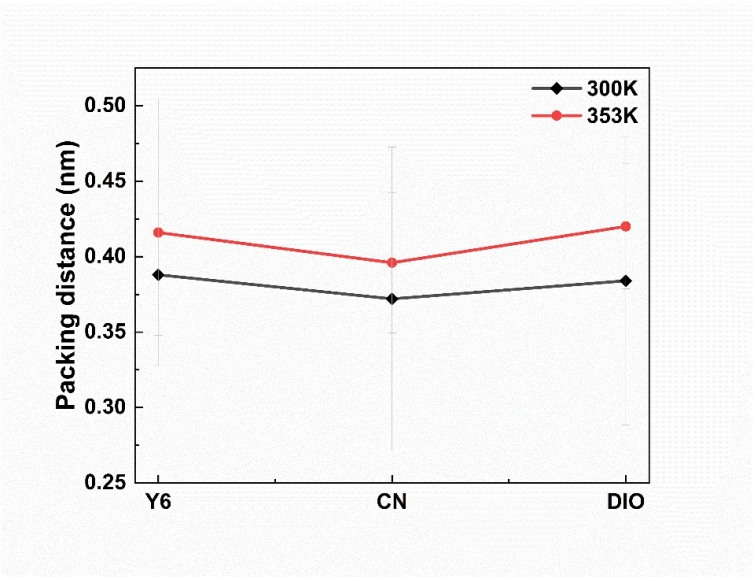

Figure S24. Calculated packing distances for Y6 dimers (CT and TT configurations) under various additive and temperature conditions.

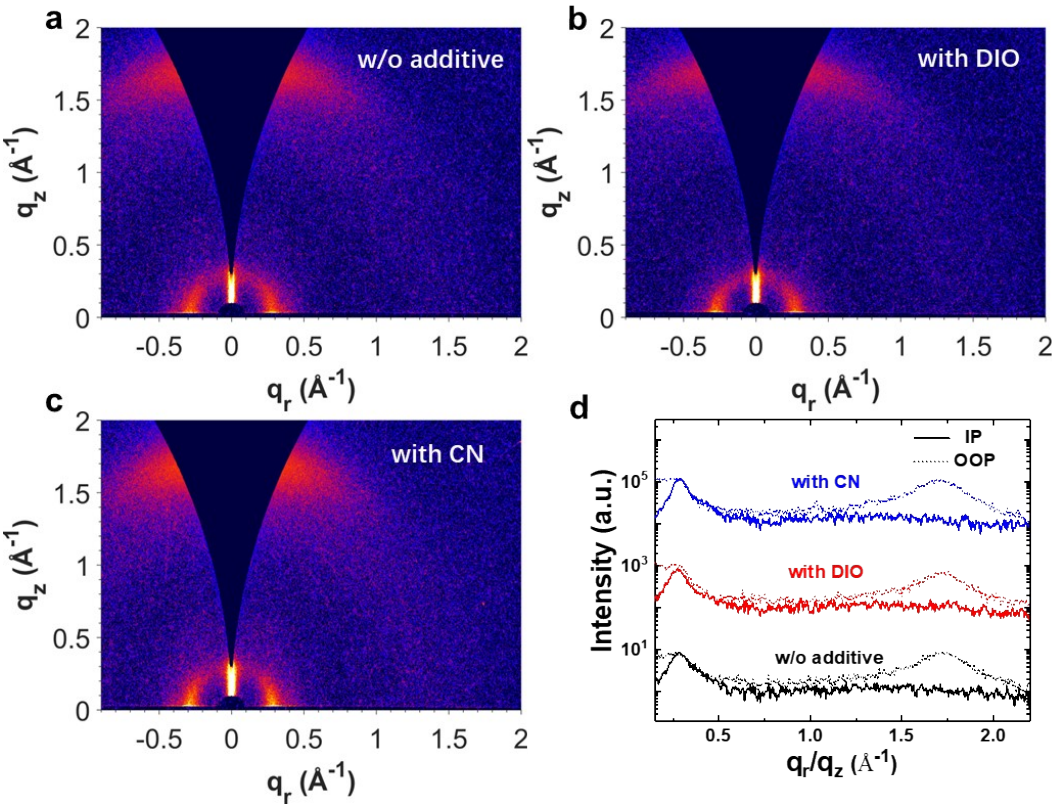

Figure S25. 2D GIWAXS patterns of PM6: Y6 blend films **(a)** without additive, **(b)** with 0.5vol% DIO and **(c)** with 0.5vol% CN. **(d)** Corresponding 1D linecuts. All the films are prepared with a D/A ratio of 1:1.2 and thermal annealing at 80 °C for 10 mins.

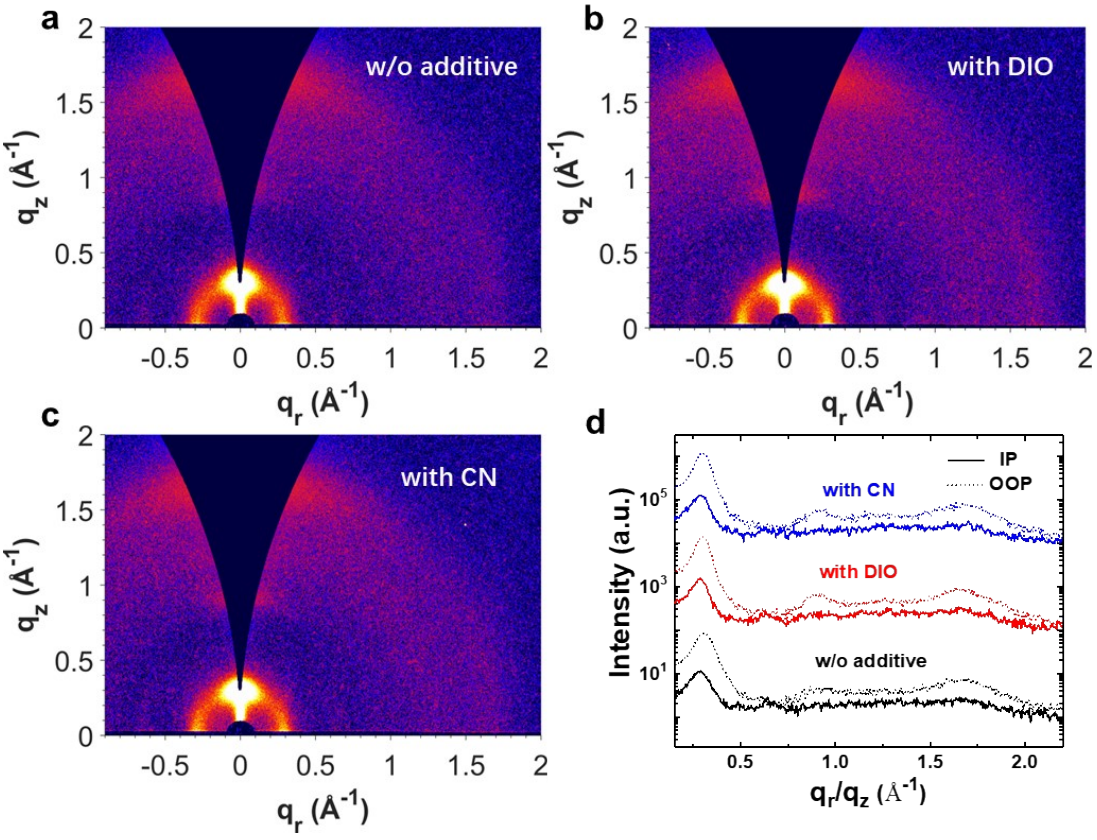

Figure S26. 2D GIWAXS patterns of PM6 neat films **(a)** without additive, **(b)** with 0.5vol% DIO and **(c)** with 0.5vol% CN. **(d)** Corresponding 1D linecuts. All the films are thermally annealed at 80 °C for 10 mins.

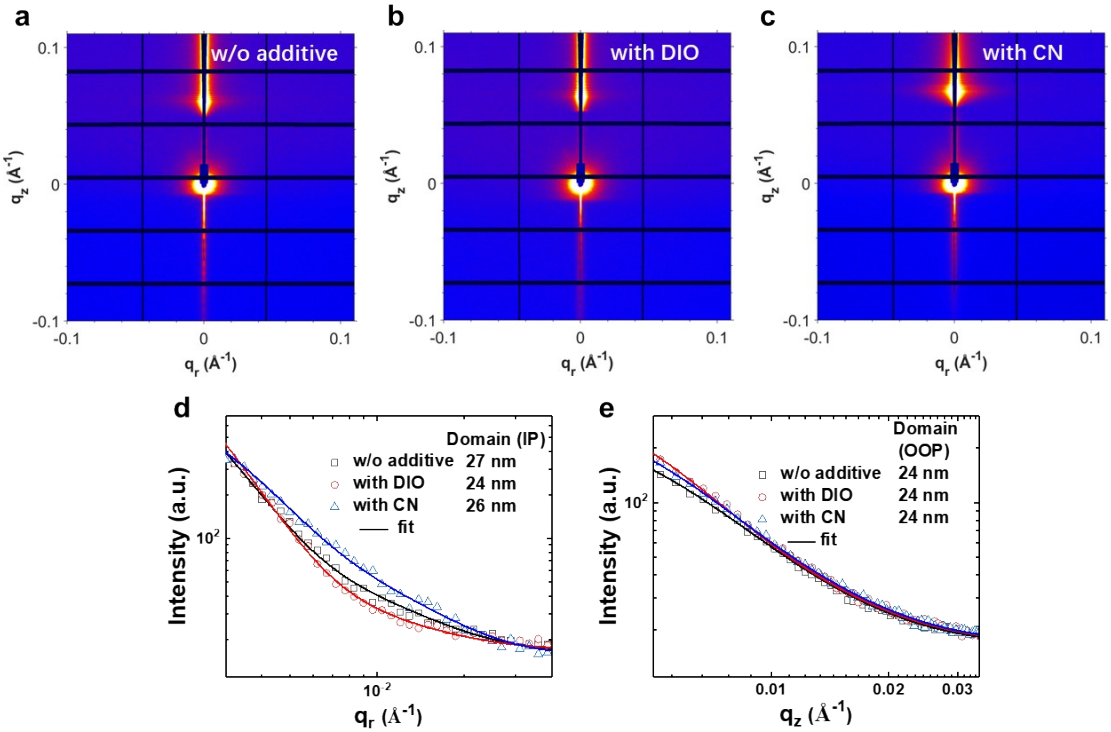

Figure S27. GTSAXS patterns of PM6:Y6 blend films annealed at 80 ℃ for 10 mins: **(a)** without additive, **(b)** with 0.5vol% DIO and **(c)** with 0.5vol% CN. Corresponding linecuts and fitting results along **(d)** IP and **(e)** OOP directions.

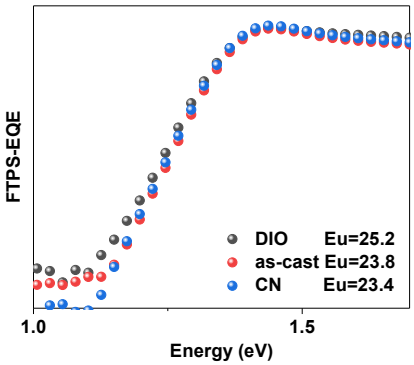

Figure S28. FTPS-EQE curves of OPVs based on PM6:Y6 blends processed with various additive conditions. The Urbach energies (E_u, meV) are derived through exponential fitting.

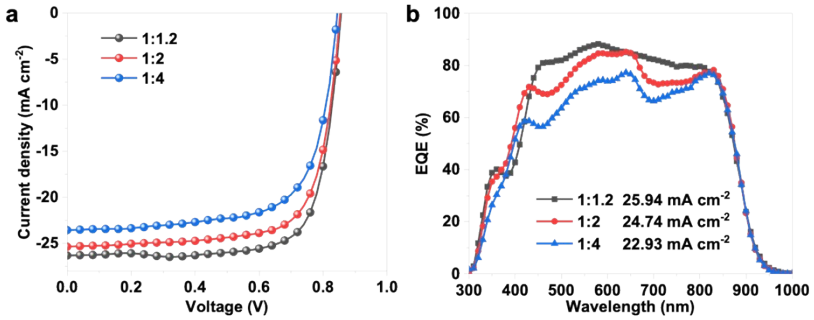

Figure S29. (a) J-V curves of OPVs based on PM6:Y6 blend films with various D/A ratios, **(b)** corresponding EQE curves.

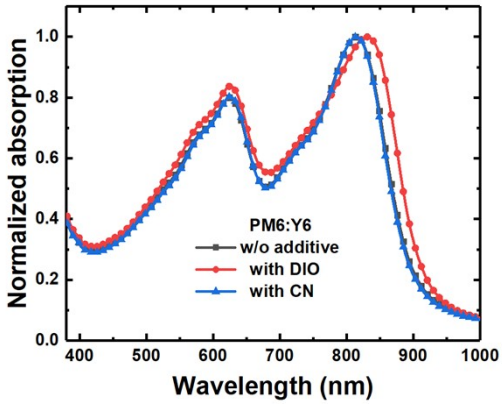

Figure S30. Normalized absorption spectra of PM6:Y6 blend films processed with various additive conditions.

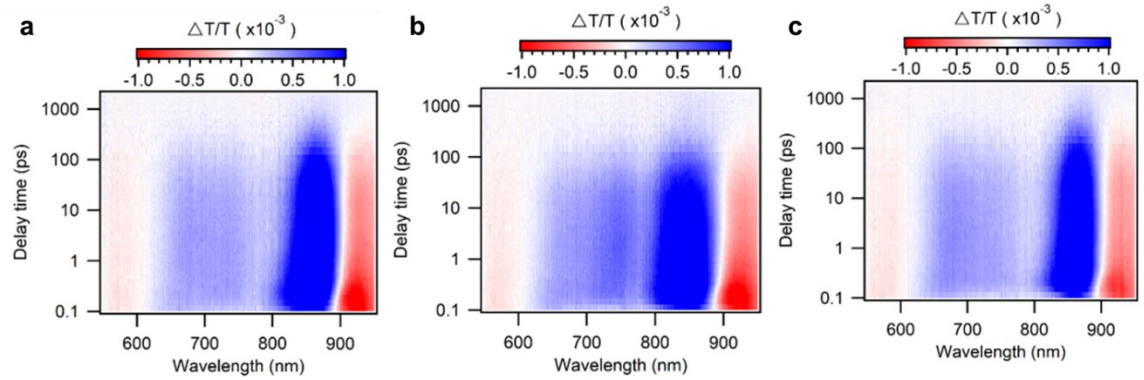

Figure S31. Color plots of the TA spectra for Y6 neat films **(a)** without additive, **(b)** with 0.5vol%DIO and **(c)** with 0.5vol% CN under 750 nm excitation.

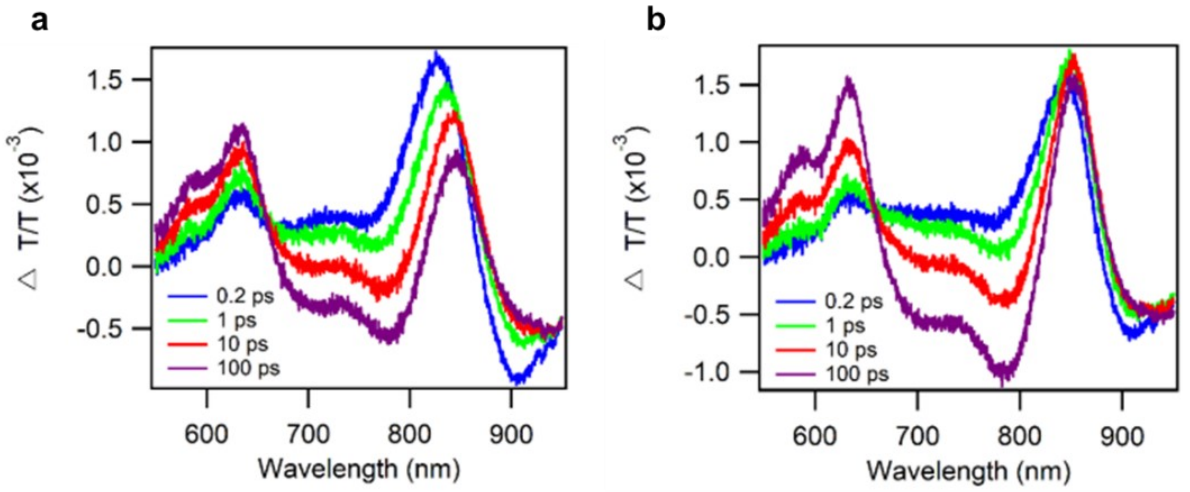

Figure S32. TA spectra at various delay times for PM6:Y6 blend films **(a)** without additive and **(b)** with 0.5vol% DIO.

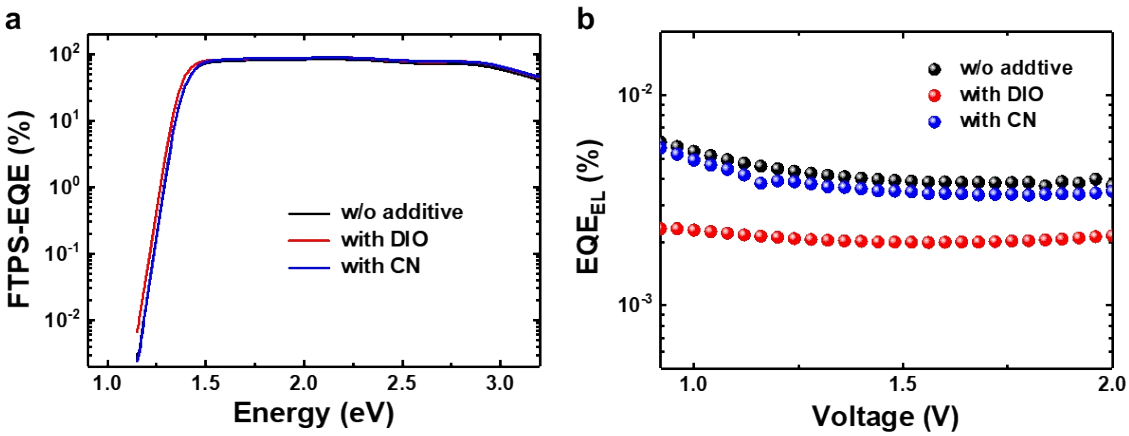

Figure S33. (a) FTPS-EQE curves of OSCs based on PM6:Y6. **(b)** EQE_{EL} of relevant OSCs at various bias voltages.

Table S1. Number of dimer configurations of Y6 under various conditions. [a]

	T-T	T-C	C-C	Others	Total
Y6 300 K	293	131	59	58	541
Y6 353 K	310	141	58	60	569
CN 300 K	357	158	35	112	662
CN 353 K	356	175	44	108	683
DIO 300 K	336	174	15	131	656
DIO 353 K	396	167	27	141	731

Table S2. Proportions of dimer configurations of Y6 under various conditions.

	T-T	T-C	C-C	Others	Total
Y6 300 K	0.54	0.24	0.11	0.11	1
Y6 353 K	0.54	0.25	0.10	0.11	1
CN 300 K	0.54	0.24	0.05	0.17	1
CN 353 K	0.52	0.26	0.06	0.16	1
DIO 300 K	0.51	0.27	0.02	0.20	1
DIO 353 K	0.54	0.23	0.04	0.19	1

[a] The simulation time is 65 ns for all systems under different temperatures, and all results were analyzed from the last ten nanoseconds (55-65 ns) from the trajectories of MDs with varying temperatures of annealing. The parameters of MDs could be obtained from the methodology.

Table S3. MDS and experimental values (extracted from **Figure S2**) of π- π stacking distance for Y6 under various additive conditions at 300 K.

	without additive	w/ CN	w/ DIO
Simulation (nm)	0.388±0.06	0.372±0.1	0.384±0.1
Experiment (nm)	0.359	0.342	0.360

Table S4. Crystalline parameters of Y6 pure films and PM6:Y6 blend films calculated from GIWAXS (**Figure S1 and S24**).

	Additive	π-π stacking			
		Q (Å^{-1})	D (Å)	FWHM (Å^{-1})	CCL (Å)
Y6	w/o	1.74	3.6	0.26	22.5
	DIO	1.74	3.6	0.22	26.6
	CN	1.77	3.5	0.22	26.6
PM6:Y6	w/o	1.71	3.7	0.26	22.5
	DIO	1.71	3.7	0.24	24.3
	CN	1.71	3.7	0.24	24.3

Table S5. Device parameters of OSCs based on PM6:Y6 blends with various D/A ratios.

D/A ratios	Voc (V)	Jsc (mA/cm^2)	Jsc cal (mA/cm^2)	FF (%)	PCE (%)
1:1.2	0.856	26.35	25.94	75.95	17.13
1:2	0.853	25.39	24.74	72.77	15.76
1:4	0.845	23.58	22.93	69.27	13.80

Table S6. Detailed energy losses of OSCs based on various PM6:Y6 blends.

Devices	E_g (eV)	qV_{oc}^{SQ} (eV)	qV_{oc}^{rad} (eV)	ΔE_1 (eV)	ΔE_2 (eV)	ΔE_3 (eV)	E_{loss} (eV)	EQE_{EL} (%)
w/o additive	1.400	1.131	1.087	0.269	0.044	0.252	0.565	0.006
with DIO	1.385	1.123	1.071	0.262	0.052	0.278	0.592	0.002
with CN	1.405	1.139	1.090	0.266	0.049	0.254	0.569	0.006

Note S1:

The total energy loss E_{loss}, which represents the energy difference between band gap (Eg) of BHJ and qV_{oc}, can be divided into three parts based on a detailed balance model [5]:

$$E_{loss} = E_g - qV_{OC} = \left(E_g - qV_{OC}^{SQ}\right) + q\left(V_{OC}^{SQ} - V_{OC}^{rad}\right) + q\left(V_{OC}^{rad} - V_{OC}\right) = \Delta E_1 + \Delta E_2 + \Delta E_3$$

where V_{OC}^{SQ} is the maximum voltage based on ideal Shockley-Quessier limit and stepwise external quantum efficiency (EQE), and V_{OC}^{rad} is the open circuit voltage when there is only radiative recombination. ΔE_1 and ΔE_2 are the radiative recombination loss above and below the bandgap, respectively. ΔE_3 is nonradiative recombination loss and can be easily calculated by $-kTln(EQE_{EL})$[6], where k is Boltzmann constant, T is Kelvin temperature, and EQE_{EL} is the electroluminescence EQE.

References

[1] Zhang, G., et al. Delocalization of exciton and electron wavefunction in non-fullerene acceptor molecules enables efficient organic solar cells. Nat. Commun. 11, 3943, (2020).

[2] Zhu, L., et al. Efficient Organic Solar Cell with 16.88% Efficiency Enabled by Refined Acceptor Crystallization and Morphology with Improved Charge Transfer and Transport Properties. Advanced Energy Materials 10, 1904234 (2020).

[3] Cui, Y., et al. Over 16% efficiency organic photovoltaic cells enabled by a chlorinated acceptor with increased open-circuit voltages. Nature communications 10.1: 2515 (2019).

[4] Zhang, Y., et al. An Electron Acceptor Analogue for Lowering Trap Density in Organic Solar Cells. Adv. Mater. 2021, 2008134.

[5] Shockley, W., et al. Detailed balance limit of efficiency of p-n junction solar cells. J. Appl. Phys. 32, 510-519 (1961)

[6] Qian D., et al. Design rules for minimizing voltage losses in high-efficiency organic solar cells. Nat. Mater. 17, 703-709 (2018)